than the phonon contribution, above $0.3\theta_D$. Therefore, it can be argued that the electronic contribution to the thermal expansion is negligible. If the lattice specific heat is used, the γ's vary more with temperature, but the shapes of the curves remain the same. If the C_e correction is based upon the work of Kneip *et* at.,[20] $\gamma_V=1.01\pm0.08$, $\gamma_a=0.94\pm0.05$, and $\gamma_c=1.20\pm0.16$ between 100 and 1130°K. If it is based upon Shimizu and Kalsuki's data,[21] $\gamma_V=1.08\pm0.15$, $\gamma_a=1.00\pm0.11$, and $\gamma_c=1.29\pm0.25$ in the same temperature range.

ACKNOWLEDGMENT

The authors would like to thank L. J. Nowicki for his assistance in a portion of the experimental work and in the various mathematical treatments of the data.

PHYSICAL REVIEW VOLUME 144, NUMBER 2 15 APRIL 1966

Empirical Fermi-Surface Parameters for W and Mo†

D. M. SPARLIN* AND J. A. MARCUS
Northwestern University, Evanston, Illinois
(Received 17 November 1965)

Torsion measurements have been made of the de Haas–van Alpen effect in tungsten and molybdenum. The results of these measurements are extremal cross-section areas of the Fermi surface and their corresponding cyclotron effective masses. These data are shown to be qualitatively interpretable in terms of orbits assigned to the various sheets of a Fermi-surface topology proposed by Lomer. A semiquantitative Fermi-surface model based on the Lomer topology is constructed and is shown to be compatible with the compensation of carriers, the connectivity of surfaces, the total surface area, the extremal dimensions, and the cyclotron effective masses reported by other investigators.

I. INTRODUCTION

THE band structure of the chromium-group metals tungsten and molybdenum is of considerable experimental and theoretical interest. Measurements of the anomalous skin effect[1] indicate that the total Fermi-surface area is much less than that for a valence-six nearly-free-electron model. Measurements of the magnetoresistance[2,3] indicate that the Fermi surface is both closed and compensated. Other experiments have determined extremal dimensions,[4,5] extremal cross-sectional areas,[6,7] and cyclotron effective masses[8,9] of the Fermi-surface sheets, often in considerable detail.

A model for the topology of the Fermi surface of the chromium-group metals which is in qualitative agreement with a majority of the above experimental results was first proposed by Lomer.[10] This model was based on

† This research was supported by grants of the National Science Foundation and the Advanced Research Projects Agency of the Department of Defense.

* Presently at Western Reserve University, Cleveland, Ohio.

[1] E. Fawcett and D. Griffiths, J. Phys. Chem. Solids **23**, 1631 (1962). Anomalous skin effect measurements on polycrystalline samples of W, Mo, and Cr show that the total Fermi surface area is much less than that for a valence-six nearly-free-electron model.

[2] E. Fawcett, Phys. Rev. **128**, 154 (1962). This paper reports kinks in the (100) magnetoresistance near ⟨100⟩ at 13° and 26° for W and at 18° for Mo. The nearly-free-electron model is shown to be inapplicable.

[3] E. Fawcett and W. A. Reed, Phys. Rev. **134**, A723 (1964). This paper reports less than 10^{-4} open cyclotron orbits per atom for Mo and less than 10^{-7} for W.

[4] J. A. Rayne, Phys. Rev. **133**, A1104 (1964); J. A. Rayne and C. K. Jones, in *Proceedings of the Ninth International Conference on Low Temperature Physics, Columbus, Ohio, 1964*, edited by J. G. Daunt, D. V. Edwards, and M. Yagub (Plenum Press, Inc., New York, 1965), p. 790.

[5] W. M. Walsh, Jr. and C. C. Grimes, Phys. Rev. Letters **13**, 523 (1964); W. M. Walsh, Jr., C. C. Grimes, G. Adams, and L. W. Rupp, Jr., in *Proceedings of the Ninth International Conference on Low Temperature Physics, Columbus, Ohio, 1964*, edited by J. G. Daunt, D. V. Edwards, and M. Yagub (Plenum Press, Inc., New York, 1965), p. 765. Their work outlines the octahedron at H and sections of the electron jack at Γ. Figure 5(c) of this paper fits their results very accurately.

[6] G. B. Brandt and J. A. Rayne, Phys. Rev. **132**, 1945 (1963). This work presents very good results for the electron lenses in Mo. Their unexplained data in the (111) plane would seem to be a result of the restriction to fields lower than 18 kG. By 25 kG in the present work it becomes clear that these frequencies are actually due to the ellpsoids at N and are exactly three times the values obtained by Brandt and Rayne [see D. M. Sparlin, thesis, Northwestern University, 1964 (unpublished)]. The Brandt and Rayne results for tungsten in the (100) plane are in excellent agreement with those reported here, with only one exception. The minima in frequency at $[\bar{1}10]$ in the (110) plane, shown by Brandt and Rayne, actually form a crossing point at $[\bar{1}10]$. This feature was only clear after study of rotation diagrams of the torque at constant field magnitude near $[\bar{1}10]$. (See Ref. 16.) The magnet used by Brandt and Rayne did not have a motor drive, thus preventing a clear definition of the symmetry. Brandt and Rayne show the "extra" terms at the ⟨100⟩ axes as do the authors' results.

[7] Private communication from R. F. Girvan and A. V. Gold. Several of the frequencies reported in this pulsed field work in the early stages were exact second harmonics of the authors' dHvA results. Since Walsh *et al.* reported nearly isotropic masses near 0.5, these apparent second harmonic terms were interpreted as their fundamentals. The authors are indebted to R. F. Girvan and A. V. Gold for their paper prior to publication.

[8] W. M. Walsh, Jr., Phys. Rev. Letters **12**, 161 (1964) and private communication.

[9] W. M. Walsh, Jr., and E. Fawcett, Bull. Am. Phys. Soc. **8**, 247 (1963).

[10] W. M. Lomer, Proc. Phys. Soc. (London) **80**, 489 (1962). This is the original proposal for the topology of a group VI transition metal Fermi surface.

a qualified assumption as to the *s-d* spacing of the energy bands of the chromium group (Cr, Mo, W) as compared with that of iron. Lomer has since revised this model to give greater detail concerning the geometry of the various sheets.[11] Mattheiss has calculated energy-band diagrams for these metals using an augmented-plane-wave technique which gives a Fermi-surface topology and geometry similar to that of the revised Lomer model.[12]

It is the primary purpose of this paper to present experimental information about the Fermi surface of tungsten and molybdenum as obtained from moderate field torsion measurements of the de Haas–van Alphen (dHvA) effect. Since a detailed description of the dHvA effect is available elsewhere,[13] suffice it to say that oscillations periodic in the reciprocal of the magnetic field appear in the susceptibility of single crystals of sufficient purity, at low temperatures, and in intense magnetic fields. The period of oscillation is related to the reciprocal of an extremal cross section of area of the Fermi surface, taken normal to the direction of the applied field. The effective mass for a particular orbit of area A_m can be determined from the temperature dependence of the amplitude of the dHvA oscillations.[13]

The secondary purpose of this paper is to show that these data may be interpreted as originating from orbits on the various sheets of the revised Lomer model. Simple solid figures are employed in determining first-order geometrical parameters for the various Fermi-surface sheets. The resulting semiquantitative models of the Fermi-surface sheets for tungsten and for molybdenum are shown to be compatible with the compensation of carriers,[3] connectivity of surfaces,[3,4] total surface area,[1] extremal dimensions,[6,7] and cyclotron effective masses[8,9] reported by other investigators.

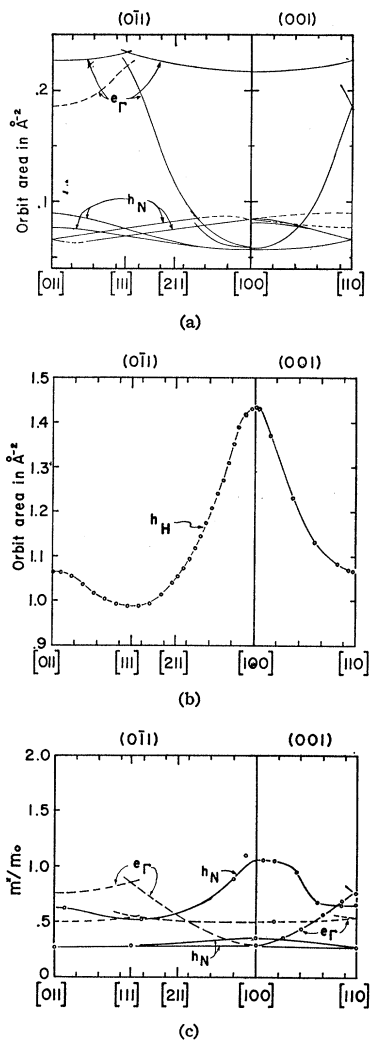

FIG. 1. (a) Tungsten. Extremal orbit areas in Å^{-2} in k space for the (0$\bar{1}$1) and (001) planes. These areas are associated with the hole ellipsoids at $N(h_N)$ and the neck and spheroid sections of the electron surface (jack) at $\Gamma(e_\Gamma)$. (b) Extremal orbit areas in Å^{-2} in k space for the (0$\bar{1}$1) and (001) planes. These areas are associated with the hole octahedron at $H(h_H)$. (c) Cyclotron effective masses (normalized to m_0) associated with the areas of Figs. 1(a) and 1(b). The masses were obtained by graphical determination of the exponential dependence of dHvA amplitude on the temperature. The limit of error is less than 10% for all points.

II. EXPERIMENTAL DETAILS

Apparatus

The sample torque was measured with a null-deflection torsion balance[14] over a field range of 0 to 34 kG. The 11 in. electromagnet (3 in. pole tips, $\frac{7}{8}$ in. gap) provided for linear sweeps in the magnet current and/or in the azimuthal angle of the field. Either the magnet current or the azimuthal angle was recorded on the x axis of an x-y recorder and the sample torque recorded on the y axis. The magnet was calibrated by using a NMR probe-frequency counter to determine B and a potentiometer and precision shunt to determine the magnet current.[14]

Samples

The tungsten samples[15] used in these measurements had residual resistance ratios (RRR) ranging from 3000 to 25 000. The RRR's for the molybdenum samples were considerably lower at 1000 to 2500. The samples were oriented to within $\pm 1°$ of the desired torque axis using a Laue x-ray technique and then epoxied to a 1-mm quartz suspension rod.

Procedures

Extensive use was made of time differentiation of the torsion balance output in order to enhance the higher frequency dHvA terms with respect to the lower ones.

[11] W. M. Lomer, Proc. Phys. Soc. (London) **84**, 327 (1964). This paper gives greater detail for the Fermi surface geometry.

[12] L. F. Mattheiss (private communication); Phys. Rev. **139**, A1893 (1965).

[13] D. Shoenberg, *Progress in Low Temperature Physics*, edited by J. C. Gorter (North-Holland Publishing Company, Amsterdam, 1957), Vol. II, pp. 226–265. The period of the free-energy oscillations is shown to be: period $(G^{-1})=2\pi eh/cS_m=9.57\times10^7/A_m$, where A_m is the extremal area in wave-number space. The effective mass is $2\pi m^*=\hbar^2 dA_m/dE$.

[14] J. H. Condon, Ph.D. thesis, Northwestern University, 1963 (unpublished); J. H. Condon and J. A. Marcus, Phys. Rev. **134**, A446 (1964).

[15] The high-purity tungsten (RRR=25 000) and molybdenum (RRR=2500) crystals were graciously provided by Bell Telephone Laboratories. Other samples were purchased from Materials Research Corp., Orangeburg, New Jersey.

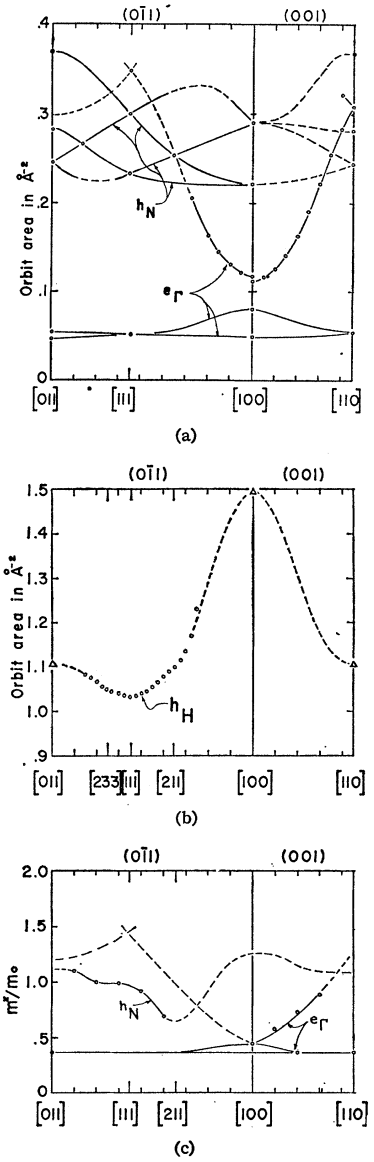

FIG. 2. (a) Molybdenum. Extremal orbit areas in Å^{-2} in k space for the (0$\bar{1}$1) and (001) planes. These areas are associated with the hole ellipsoids at $N(h_N)$, the neck section of the electron surface (jack) at $\Gamma(e_\Gamma)$, and the electron lenses along the ΓH lines ($e_{\Gamma H}$). (b) Extremal orbit areas in Å^{-2} in k space for the (001) and (0$\bar{1}$1) planes. These areas are associated with the hole octahedron at $H(h_H)$. The dashed line is an extrapolation of the observations assumming an octahedral geometry for the surface. (c) Cyclotron effective masses (normalized to m_0) associated with the areas of Figs. 2(a) and 2(b). The masses were obtained by graphical determination of the exponential dependence of dHvA amplitude on the temperature.

Differentiation was applied not only when recording the sample torque as a function of the magnet current, but also while recording the torque at constant magnetic-field strength as a function of the angle between the applied field and the crystal axes. Such rotation diagrams, both direct and differentiated, are extremely useful since an oscillation in the dHvA torque is observed whenever the frequency $f(\theta)$ changes by the value of the steady applied field B_0.[16]

Values for the effective masses of the different extremal orbits were obtained from the temperature variation of the dHvA amplitudes at a fixed applied field.[13] Both rotation diagrams and field-sweep curves

[16] The importance of the rotation diagrams in defining the nature of the symmetry points in the area versus angle plots was first pointed out to the authors by J. H. Condon.

TABLE I. Summary of dHvA data for W and Mo.

Plane	Direction	Area (Å^{-2})	M^*	Assignment of orbit
		Tungsten		
(001)	[100]	0.0573	0.28	hN Ellipsoid
		0.058	0.29	$e\Gamma$ Neck
		0.0815	0.365	hN Ellipsoid
		0.0850	0.365	hN Ellipsoid
		0.2175	0.505	$e\Gamma$ Spheroid
		1.436	1.06	hH Octahedron
	[110]	0.066	0.276	hN Ellipsoid
		0.0772		hN Ellipsoid
		0.0903		hN Ellipsoid
		0.186	0.75	$e\Gamma$ Neck
		0.228		$e\Gamma$ Spheroid
		1.067	0.65	hH Octahedron
(0$\bar{1}$1)	[100]	0.0577		hN Ellipsoid
		0.0584	0.307	$e\Gamma$ Neck
		0.0815	0.354	hN Ellipsoid
		0.2175		$e\Gamma$ Spheroid
		1.436	1.11	hH Octahedron
	[111]	0.0692	0.287	hN Ellipsoid
		0.076	0.287	hN Ellipsoid
		0.236		$e\Gamma$ Spheroid
		0.2235		$e\Gamma$ Neck
		0.99	0.52	hH Octahedron
	[011]	0.0665	0.262	hN Ellipsoid
		0.0772		hN Ellipsoid
		0.0900		hN Ellipsoid
		0.228		$e\Gamma$ Sphere
		1.067	0.63	hH Octahedron
($\bar{1}$11)	[110]	0.0665		hN Ellipsoid
		0.0766		hN Ellipsoid
		0.0903		hN Ellipsoid
	[211]	0.0617		hN Ellipsoid
		0.0638		hN Ellipsoid
		0.0742		hN Ellipsoid
		0.0797		hN Ellipsoid
		Molybdenum		
(001)	[100]	0.0498		$e\Gamma H$ Lens
		0.0786	0.43	$e\Gamma H$ Lens
		0.1125	0.42	$e\Gamma$ Neck
		0.22		hN Ellipsoid
		0.298		hN Ellipsoid
	[110]	0.0485		$e\Gamma H$ Lens
		0.055	0.37	$e\Gamma H$ Lens
		0.250	0.34	hN Ellipsoid
		0.267		hN Ellipsoid
		0.308		$e\Gamma$ Neck
		0.325		
		0.383		hN Ellipsoid
(0$\bar{1}$1)	[100]	0.0509		$e\Gamma H$ Lens
		0.0815	0.445	$e\Gamma H$ Lens
		0.1175	0.445	$e\Gamma$ Neck
		0.22		hN Ellipsoid
		0.297		hN Ellipsoid
	[111]	0.052		$e\Gamma H$ Lens
		0.2335		hN Ellipsoid
		0.295		hN Ellipsoid
		0.348		$e\Gamma$ Neck
		1.037	0.95	hH Octahedron
	[011]	0.0473		$e\Gamma H$ Lens
		0.054		$e\Gamma H$ Lens
		0.246	0.366	hN Ellipsoid
		0.282		hN Ellipsoid
		0.294		$e\Gamma$ Neck
		0.368		hN Ellipsoid

were utilized in sorting the observed torque into its various component amplitudes at each temperature.

III. EXPERIMENTAL RESULTS

The results of the measurements are presented as Figs. 1(a) through 2(c) and Table I.[17] The over-all accuracy of Table I is better than 2%. The solid lines represent direct observations, smoothly joined for clarity. The dashed lines are extensions of the data in a manner compatible with the requirements of crystal symmetry.

Any discussion of a purely empirical nature has been relegated to the figure captions or to footnotes. Comparisons made between the detailed observations of other investigators and those reported here have been included in the relevant footnote.

IV. INTERPRETATION OF RESULTS

The Fermi-surface model proposed by Lomer for the chromium-group bcc metals tungsten and molybdenum consists of the following surfaces, shown schematically for the (001) plane in Fig. 3:

(1) Six hole ellipsoids, whose major axes may be along either ⟨100⟩ or ⟨110⟩, are located at the points N in the Brillouin zone.

(2) A hole octahedron is centered on the symmetry point H of the Brillouin zone.

(3) An electron surface is centered on Γ and may be considered to be formed by an octahedron at Γ which intersects six prolate spheroids lying along the ΓH directions (a figure not unlike a child's jack).

(4) Six electron lenses, which are formed by the intersection of the prolate spheroids and the rounded points of the octahedron, lie along the ΓH lines and are inside the "necks" of the electron jack.

An interpretation of Figs. 1 and 2 in the terms of the surfaces defined in (1) through (4) is presented in the following paragraphs.

A. Hole Ellipsoids at N

Molybdenum

Identification of the dHvA oscillations due to orbits on the various hole ellipsoids was accomplished by a comparison of the observed angular variation of areas with the requirements of crystal symmetry at the point N. For example, $dA/d\theta \neq 0$ at [011] in the $(0\bar{1}1)$ plane is required by a set of ellipsoids at N but not by prolate spheroids lying along the ⟨100⟩ axes. The areas labeled holes at $N(hN)$ in Fig. 2(a) were identified by this feature.[6] The major axes of the ellipsoids are found to lie along ⟨100⟩ from the ordering of zero and nonzero values of $dA/d\theta$ at the ⟨110⟩ and ⟨100⟩ axes.

[17] The units are reciprocal angstroms in wave-number space $(2\pi/a)$, and m^* is normalized to m_0, the free-electron mass.

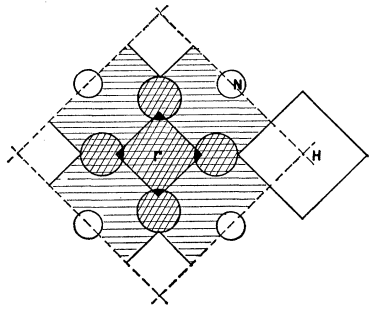

FIG. 3. Theoretical topology of the Fermi surface of nonmagnetic chromium, molybdenum, and tungsten. Spin-dependent interactions have not been included. [After W. M. Lomer, Ref. 11.]

Having identified those data corresponding to various orbits on the ellipsoids, a calculation of the three semimajor axes yields[18]:

$$a=0.39\pm0.01\ \text{Å}^{-1};\quad b=0.30\pm0.01\ \text{Å}^{-1};$$
$$c=0.23\pm0.01\ \text{Å}^{-1}.$$

If the relevant energy bands have a quadratic expansion of the form

$$E(k)=k_x^2/A+k_y^2/B+k_z^2/C$$

near the Fermi energy E_F, band maxima for the hole ellipsoids may be defined such that the energy difference between the Fermi energy E_F and the energy at the band maxima E_N is given by $E_N-E_F \propto A/m^*$. The results for a ⟨110⟩ field direction yield $(E_N-E_F)=0.81\pm0.05$ eV. The total volume of such six hole ellipsoids is ≈ 0.71 Å^{-3}, and their surface area is ≈ 7.2 Å^{-2}.

Tungsten

The identification of the ellipsoid areas in the tungsten data was difficult due to their smaller eccentricity. The crossing of the $A(\theta)$ curves at [011] in the $(0\bar{1}1)$ plane could not be uniquely demonstrated from the results of the field-sweep data. However, rotation diagrams of the torque as a function of angle at constant magnetic field strength demonstrated both the presence of the crossing $(dA/d\theta \neq 0)$ and area extremals ±10 deg to either side of the [011] axis.[16] Those areas due to hole ellipsoids at N in tungsten are shown in Fig. 1(a).

The semimajor axes of these ellipsoids are calculated to be: $a=0.195\pm0.002$ Å^{-1}, $b=0.146\pm0.002$ Å^{-1}, and $c=0.125\pm0.002$ Å^{-1}.[19] The major axes (again) lie parallel to the ⟨100⟩ directions in the {110} zone faces.

Both the dHvA area and its related cyclotron effective mass were determined for a number of extremal orbits on these surfaces in tungsten.[20] This makes it possible to demonstrate that these surfaces are closely ellipsoidal. The data are shown in Table II. Thus $E(k)$ for the holes at N in tungsten is quadratic near E_F and

[18] The extremal areas viewed along the axes a, b, and c are $A_a=0.220$ Å$^{-2}=\pi bc$; $A_b=0.282$ Å$^{-2}=\pi ac$; $A_c=0.368$ Å$^{-2}=\pi ab$.

[19] The extremal areas viewed along the axes a, b, and c are $A_a=0.0573$ Å^{-2}; $A_b=0.0772$ Å^{-2}; and $A_c=0.0900$ Å^{-2}.

[20] The presence of the "neck" term in the already complicated structure due to the ellipsoids at N in molybdenum prevented any attempt at determining the degree of ellipsoidicity in this case.

TABLE II. Data on hole ellipsoids in tungsten.

Plane	Direction	$1.2A/m^*=(E_N-E_F)$ (eV)
(001)	[100]	1.2(0.0815/0.365)=0.269 eV
	[100]	1.2(0.0850/0.365)=0.280 eV
	[011]	1.2(0.066/0.276)=0.287 eV
(0$\bar{1}$1)	[100]	1.2(0.0815/0.354)=0.276 eV
	[111]	1.2(0.0692/0.287)=0.288 eV
	[011]	1.2(0.0665/0.262)=0.305 eV
		6/1.705 eV
		$(E_N-E_F)=0.284\pm0.02$ eV

E_F lies 0.284 ± 0.02 eV below E_N. The volume of these six ellipsoids is ~0.089 Å^{-2} and their total surface area is ~1.70 Å^{-2}.

B. Hole Octahedron at H

Tungsten

The dHvA results shown in Fig. 1(b) display the symmetry of point H, and approximate those for an octahedral Fermi-surface sheet.[5,7] If this approximation is adopted, the edge length l may be estimated from the extremal cross section area at the ⟨111⟩, ⟨100⟩, and ⟨0$\bar{1}$1⟩ orientations of applied field. The mean edge length l is found to be 1.22 Å^{-1}.[21] The octahedron volume is then $\cong5.3$ Å^{-2}.

The hole octahedron dHvA amplitudes were continuous and smoothly varying with magnet angle for all orbits, in particular for **B** near a ⟨100⟩ axis. This implies that no carriers were lost from these orbits through transitions onto another sheet. While this is not sufficient evidence, it is in agreement with magnetoresistance studies[3] which disclose no open orbits in these metals. In addition, recent magnetoacoustic[4] and size effect[5] studies show that the hole octahedron at H in tungsten does not contact the electron "jack" along the line ΓH.

The variation of the effective mass with orientation of the applied field is displayed in Fig. 1(c). These values are in agreement with those determined by Azbel-Kaner cyclotron resonance.[8]

Molybdenum

The experimental results showing the symmetry required by the holes at H are found in Fig. 2(b). The points designated by 0 near the ⟨111⟩ direction represent the data of this paper, while the triangles (△) at the symmetry axes [100] and [110] are due to the pulsed-field dHvA measurements[7] of other investigators. The dashed line connecting the two sets of data points is a plausible extrapolation if it is assumed that these data are associated with the holes at H.

Following this assumption, the length of the edge of the octahedron is estimated from the extremal area along ⟨111⟩ as $l\cong1.264$ Å^{-1}.[22] The volume is then $\cong0.95$ Å^{-3} and the surface area is $\cong5.5$ Å^{-2}.

The effective masses associated with the extremal areas of Fig. 2(b) are shown in Fig. 2(c). The ripples in the area plot for field orientations near [233] and [211] are seen to be reproduced in the effective-mass plot.

Although the interpretation of the data in Fig. 2(b) as due to holes at H can lead to no serious inconsistancies, there are alternative interpretations. If these data were due to body orbit electrons at Γ, the observed loss of dHvA amplitude $\approx10°$ from [110] in the (0$\bar{1}$1) plane would correspond to the intersection of the orbit path with the neck in the jack arm. A magnetoresistance kink was observed 18° from [100] in the (001) plane.[2] This 8° difference supports the identification of the observed dHvA data with the holes at H (hole octahedron).[23]

C. Electrons at Γ

Tungsten

The minimum in area observed in tungsten (Fig. 1(a)) is readily identified with the neck between the jack body and the intersecting spheroids. If the fourfold symmetry along a ⟨100⟩ axis is assumed to be satisfied by small deviations from cylindrical symmetry, a radius for the neck is $P_n=0.136$ Å^{-1}. Since the neck orbit was observed at a ⟨111⟩ orientation of field, the octahedron taken as the first approximation for the body of the jack must be concave along the ⟨111⟩ axes.

The values of the effective mass for the neck orbits are shown in Fig. 1(c). The associated amplitudes are quite strong in the torsion dHvA data but apparently contribute only weakly to cyclotron-resonance experiments since they have not been reported.[8]

The dHvA torque amplitude for these neck orbits does not vanish when $m^*=0.5$, as opposed to the behavior of the necks in copper.[24] This implies the existance of appreciable spin-orbit coupling. According to the Lifshitz-Kosevich theory[25] for the dHvA effect, the amplitude of the lth harmonic will vanish when the spin-splitting factor $\cos[(l/2\pi m_0)(dS/dE)]$ is zero. Cohen and Blount[26] pointed out that when spin-orbit coupling is important, the spin-splitting factor in the Lifshitz-Kosevich theory should be generalized to $\cos\frac{1}{2}(\pi lgm^*)$, where g, the electron g factor, can differ appreciably from the value of 2. In this instance, since

[21] From Table I: $A_{111}=0.99$ Å$^{-2}=\rangle l=1.234$ Å^{-1}; $A_{110}=1.067$ Å$^{-2}=\rangle l=1.23$ Å^{-1}; $A_{100}=1.436=\rangle l=1.2$ Å^{-1}. The average value for l will be used in the calculation of the volume and surface area of the octahedron used as a semiquantitative model.

[22] The extremal area viewed along ⟨111⟩ is $A_{111}=1.037$ Å^{-2}.

[23] In fact, the compensation of holes and electrons in both tungsten and molybdenum (see Refs. 2, 3) requires that the hole octahedron and the body of the electron jack must be nearly the same size; thus these experimental observations [Fig. 4(b)] may turn out to be an unresolved sum of the contributions from both surfaces.

[24] A. S. Joseph and A. C. Thorsen, Phys. Rev. **134**, A979 (1964). An example of the dHvA amplitude vanishing for $m^*=0.5$ is given here.

[25] I. M. Lifshitz and A. M. Kosevich, Zh. Eksperim. i Teor. Fiz. **29**, 633 (1955) [English transl.: Soviet Phys.—JETP **2**, 636 (1956)].

[26] M. Cohen and E. I. Blount, Phil. Mag. **5**, 115 (1960).

the amplitude is nonzero in the range $0.3<m^*<0.75$, one may set the limits $3.33<g<4$ for the neck orbit g factor in tungsten.[27]

The largest areas shown in Fig. 1(a) are slowly varying with angle as would be expected for orbits on a spheriod and their amplitudes are correspondingly weak. Since the angular variation is measurable, it is possible to estimate the major and minor axes of prolate spheroids which approximate to the data and represent the bulges on the jack. The semiminor axis is calculated from the dHvA area along a ⟨100⟩ axis[28] to be $R_s=0.263$ Å^{-1}. The semimajor axis of the spheroid is then calculated from the extrapolated value of the area at [010] to be $R_L=0.290$ Å^{-1}.

The dHvA effect arising from orbits on the spheroids was observed to persist to a ⟨111⟩ orientation of the applied field. This fact is consistent with the dimensions just calculated for the neck radius and the semimajor axis of the spheroid, since $\tan^{-1}(R_L/R_n)=64°\cong$angle at which a spheroid centered orbit would intersect the neck. This value is greater than the angle between [100] and [111].

A single value for the effective mass of an orbit on a spheroidal surface was obtained for an applied magnetic field 10 deg from [100] in the (001) plane.[29] The effective mass at this point was $m^*\cong 0.505\pm 0.01$. If $g\cong 2$, then this m^* value causes the spin-splitting factor to strongly attenuate the odd harmonic terms. Evidence of this effect is found in the dominance of second harmonics of the spheroid terms when the dHvA effect is investigated by pulse-field techniques.[7] Cyclotron resonance measurements of m^* also support a nearly isotropic mass value near 0.5.[8,9]

Oscillations corresponding to orbits centered on the body of the electron surface at Γ were not detected in this investigation. Such areas and effective masses have been determined from pulsed field dHvA[7] and cyclotron-resonance[8] measurements by other investigators however.

Extremal dimensions of the jack have been determined both by magnetoacoustic attenuation[4] and by size-effect measurements.[5] These dimensions can be utilized in the following way: the dimension from the center of the zone, Γ, to the end of the jack arm has been reported as 1.10 ± 0.01 Å^{-1}.[4,5] The results of this paper indicate that the spheroid major axis is ≈ 0.58 Å^{-1}. Thus the distance from Γ to the plane of the neck orbit is approximately $(1.10-0.58)$ Å$^{-1}=0.52$ Å^{-1}. The mean neck radius is 0.136 Å^{-1}. The body orbit centered on Γ will suffer a discontinuity when it intercepts the neck: The angle of interaction is approximately $\tan^{-1}(136/0.52)=(14.0\pm 0.5)°$. This result is in excellent agreement with the magnetoresistance data[2] which exhibits a kink in the plot of resistance versus magnetic field angle $\approx 13°$ from ⟨100⟩ in a (100) plane. Other observations of singularities near this angle substantiate this identification.[4,5,7]

The body of the jack is then approximated by an octahedron of edge length $\approx\sqrt{2}(0.52+0.136)$ Å$^{-1}\approx 0.93$ Å^{-1}. This approximation yields the body contribution to the volume as ≈ 0.38 Å^{-3}, and the body surface area as ≈ 2.9 Å^{-2}. The volume contributed by the spheroids is ~ 0.5 Å^{-3} and their surface area is ~ 5.7 Å^{-2}. The total electron-jack contribution is thus; volume ≈ 0.88 Å^{-3} and surface area ≈ 8.6 Å^{-2}.

Molybdenum

A minimum in area occurs in the molybdenum results which is readily identified as arising from a neck in the Fermi surface. If it is (again) assumed that the neck minimum orbit is nearly circular we may calculate a neck radius,[30] $R_n=0.192$ Å^{-1}.

Neck orbits were found to exist for field orientations along ⟨111⟩ in molybdenum (as was the case in tungsten). The octahedron taken as a first approximation for the body of the electron jack in molybdenum must (also) be concave along the ⟨111⟩ axes.

Effective mass values for the neck orbits were determined only in the (001) plane as shown in Fig. 2(c). The associated amplitudes were weak in relation to those from the holes at N, as compared with the case in tungsten where the neck and ellipsoid amplitudes were of the same order. This is apparently due to the higher values of m^* for neck carriers in molybdenum. The effective mass was found to vary between the limits $0.45\leqq m^*\leqq 0.9$ and the amplitude did not vanish in this range. Thus, the value of the electron g factor must lie between the limits $2.22\leqq g\leqq 3.33$.[27]

No orbits other than the neck orbits were observed for the electron jack in molybdenum. However, it is possible to estimate several of the parameters of this surface by combining the neck orbits, the lens orbits, and a kink in the magnetoresistance[2] similar to that observed in tungsten. This is done in the following section.

D. Electron Lenses Along ΓH

Molybdenum

Evidence for the existance of the electron lenses along ΓH in molybdenum is found in the lowest areas of Fig. 2(a). Previous authors[6] have pointed out that these sheets are not figures of revolution but are slightly elongated along the transverse ⟨100⟩ directions. This detail is implicit in the results presented in Table I.

[27] One sets $g=(2n+1)(1/m^*)$ in the observed range of m^* values and observes that nonvanishing amplitudes could only occur if $3.33\leq g\leq 4.0$.

[28] $\pi R_s^2=0.2175$ Å^{-2}, $R_s=0.263$ Å^{-1}. This value corresponds to a circular cross section of radius 0.26 Å^{-1} reported from magnetoacoustic attenuation experiments.[4] $\pi R_s R_1=0.239$ Å^{-2} giving $R_1=0.290$ Å^{-1}.

[29] A field sweep of the torque at this orientation was dominated at a particular field value by the spheriod term alone.

[30] $\pi R_n^2=0.115$ Å^{-2}; $R_n=0.192$ Å^{-1}.

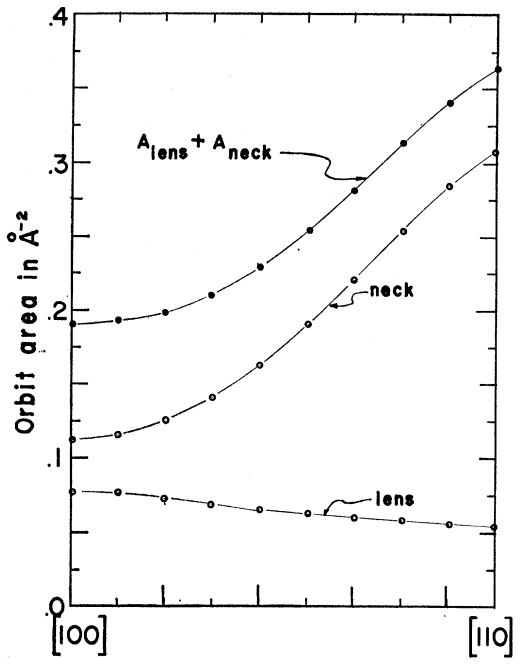

(a)

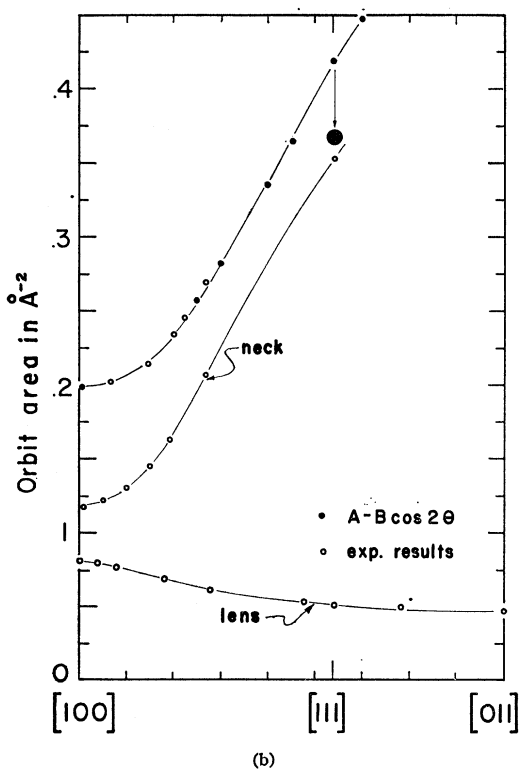

(b)

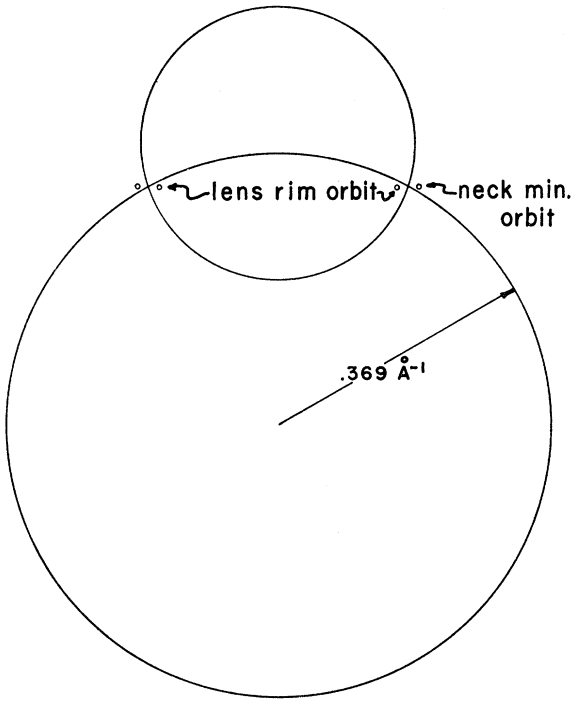

(c)

FIG. 4. (a) Molybdenum. Plot of the neck area, the lens area, and their sum. The sum area is of the form $A-B\cos 2\theta$ for a neck and lens formed by two intersecting spherical sections of the Fermi surface, provided the degeneracies are removed by small interaction terms. (b) Plot of the neck area, the lens area, and their sum. The large black dot represents the extrapolation of $A-B\cos 2\theta$ at $\langle 111\rangle$ minus the experimental lens area at $\langle 111\rangle$. The discrepancy indicates that at least one of the two spheriods is prolate. (c) Schematic diagram of the result of an iterated solution for radii and center displacements of two-sphere model for neck and lens areas.

The distortion amounts to $\sim 3\%$ in radius and satisfies the fourfold symmetry of the ΓH lines.

The amplitudes of the lens terms in the dHvA torques were smoothly varying for all orientations of the applied field. Thus, it may be concluded that the lenses are not connected with the necks by either degeneracies or magnetic breakthrough in the field range investigated.

Values for the effective mass of orbits on the lenses were determined at [100] and [110] directions of the applied field. The [100] direction of field corresponded to a rim orbit on the lens. The m^* value obtained was 0.445 and was identical to the neck-minimum orbit mass as shown in Fig. 2(c).

It has been shown that the effect of spin-orbit coupling on the tungsten energy bands is to create gaps between the electron jack and the hole octahedron and between the electron jack and the lenses.[5,31] The lens-neck energy gap is $\Delta E=1.2\Delta A/m^*=0.096\pm0.001$ eV in molybdenum.[32] This energy gap is thought to be entirely due to spin-orbit coupling.

The fact that the lens-rim orbit and neck-minimum orbit have identical values of effective mass suggests the use of two intersecting, nearly free electron spheres as a model for the region of the Fermi surface including the rounded tip of the octahedron at Γ, its intersecting spheroid, and the enclosed lens. This model has the property that the sum of the areas of the lens and neck orbits should be approximately

$$\text{Area total}=A_{\text{lens}}+A_{\text{neck}}=A_0+B_0\cos2\theta,$$

where

$$A_0=\prod\left[(R_a^2+R_b^2)-\tfrac{1}{2}(D_a^2+D_b^2)\right],$$
$$B_0=\prod\tfrac{1}{2}(D_a^2+D_b^2),$$

and

R_a = radius of curvature of the rounded end of the octahedron at Γ,

R_b = radius of sphere,

D_a = distance from center of curvature of octahedron point to plane of intersection with sphere,

D_b = distance from center of sphere to plane of intersection with octahedron.

Figure 4(a) displays a plot of the area of the lens orbit, the area of the neck orbit, and the sum of the two versus angle in the (001) plane of molybdenum. A fit of $(A_0-B_0\cos2\theta)$ to the sum at $\theta=0°$ and $\theta=25°$ gives $A_0=0.364$ Å^{-2} and $B_0=0.171$ Å^{-2}.

Figure 4(b) shows a similar plot for the $(0\bar{1}1)$ plane. The experimental points cover a range of 27° from ⟨100⟩ with an additional point at the ⟨111⟩ direction. The empirical expression fitted to the sum at $\theta=0°$ and $\theta=25°$ as before gives $A_0=0.364$ Å^{-2} and $B_0=0.165$ Å^{-2}. If these values for A_0 and B_0 are used to calculate the total area of the neck orbit plus the lens orbit at a ⟨111⟩ direction of the field, and the experimental value for the lens area is subtracted, the large black dot in Fig. 4(b) results. This point compares favorably with the experimental value for the neck area at the ⟨111⟩ orientation, at least to the order of the approximation.

The experimental value for the area of an orbit passing across a face of the lens is now set equal to the average theoretical value, written in terms of R_b alone. A value for R_b is then determined by iteration. The iteration was stopped at a calculated lens area of 0.043 Å^{-2} (experimental value=0.049 Å^{-2}) with the corresponding value of R_b equal 0.37 Å^{-1} [see Fig. 4(c)].

This rough estimate for the dimension of the sphere at the end of the jack finds support in the pulsed field dHvA data[7] through an otherwise unidentified period corresponding to a radius of 0.363 Å^{-1}.[33] Preliminary magnetoacoustic attenuation results[4] reveal a k value of ~0.3 Å^{-1} along a ⟨100⟩ direction, although this dimension may be due to the hole ellipsoids at N rather than the jack spheroids.

The magnetoresistance data[2] show a kink in the (001) rotation diagram ~18° from [100]. If it is assumed that this kink is due to the intersection or orbits centered on Γ with the neck, as was the case for tungsten, the following approximation may be made:

$$\text{Distance from } \Gamma \text{ to plane of neck} \cong \text{neck radius}/\tan18° \cong 0.59 \text{ Å}^{-1},$$

and

$$\begin{bmatrix}\text{Distance from } \Gamma \text{ to}\\ \text{end of sphere}\end{bmatrix} \cong \begin{bmatrix}\text{Distance from } \Gamma\\ \text{to plane of neck}\end{bmatrix} + \begin{bmatrix}\text{Diameter of}\\ \text{sphere}\end{bmatrix}$$
$$\cong 1.3 \text{ Å}^{-1}.$$

Preliminary magnetoacoustic attenuation results[4] have indicated a k value of 1.2 Å^{-1} along a ⟨100⟩ direction. The above estimate indicates that 1.2 Å^{-1} is indeed the length of the electron jack from Γ to the tip of the sphere.

The edge length of the octahedron taken to approximate the body of the jack is estimated as $l\approx\sqrt{2}(0.59+0.19)$ Å$^{-1}=1.1$ Å^{-1}. The volume contributed by the jack body is then ~0.63 Å^{-3} and the surface area is ~4.2 Å^{-2}. The volume contributed by the six spheroids is ~1.22 Å^{-3} and their surface area is ~10.2 Å^{-2}. The total volume enclosed by the jack and the lenses is then ≈1.8 Å^{-3} and the total surface area is ≈14.4 Å^{-2}.

Tungsten

No dHvA oscillations having the symmetry of angular variation of frequency required of the lens surfaces were observed in tungsten in this experiment. Experimentally, this implies either that the lenses are anomalously high effective-mass surfaces, are nearly isotropic in area, are prolate and hidden among the oscillations from the hole ellipsoids at N, or that the lens band (the fifth) is not occupied.

[31] L. F. Mattheiss and R. E. Watson, Phys. Rev. Letters **13**, 526 (1964).

[32] This is a rigid-band approximation which makes use of the area difference between the lens rim and the neck minimum orbits and the fact that identical values of cyclotron effective mass were found for both.

[33] It was assumed that the reported period was actually the second harmonic of the sphere equatorial orbit, as was the case in tungsten. Also, $m^*\approx0.5$ was expected for the sphere orbits in molybdenum from the cyclotron resonance work and from the apparent isomorphism of the two Fermi surfaces.

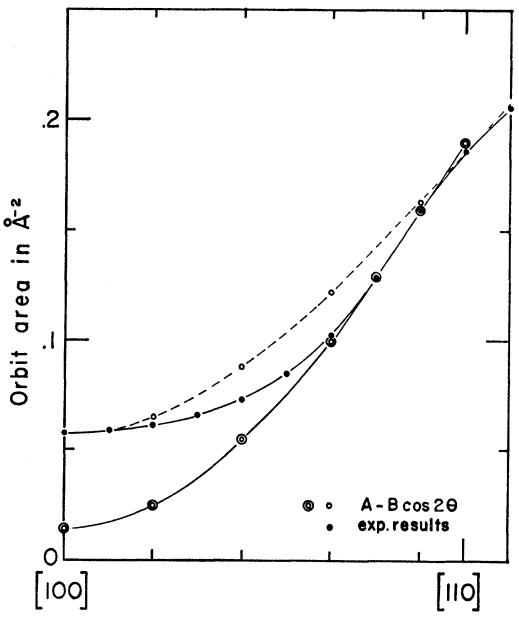

(a)

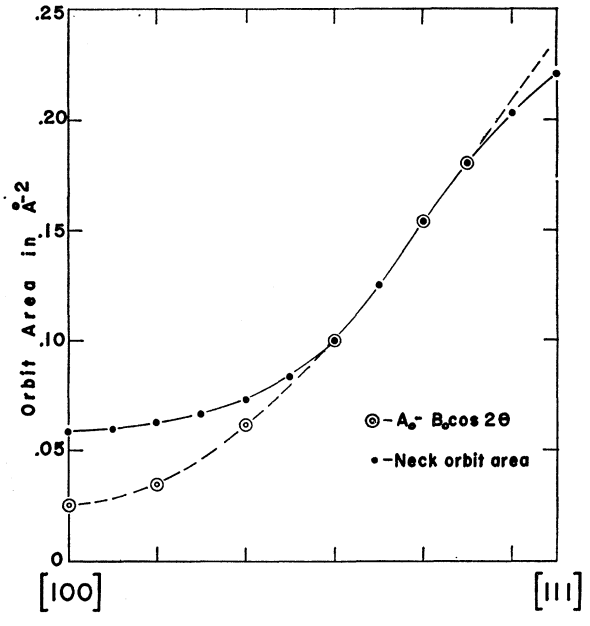

(b)

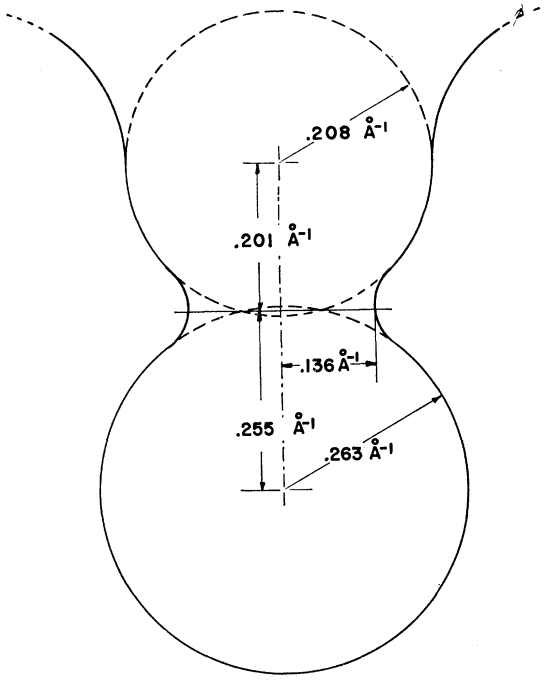

(c)

FIG. 5. (a) Tungsten. Plot of the neck area in the (001) plane. No lens surface was observed. The double open circles are a fit of the function $A-B\cos 2\theta$ to the slope of the neck data near [110]. The lens (if it exists) will contribute a slowly varying area near [110]. (b) Plot of the neck area in the (01$\bar{1}$) plane. The close similarity of the angular variation of the neck in the (01$\bar{1}$) and the (001) planes adds plausibility to the application of the two sphere model. (c) Schematic diagram of the results obtained from two-sphere model for radii and center to center distances. The neck (0.136 Å^{-2}) and spheroid (0.263 Å^{-2}) radii were calculated from experimental areas.

The first and third alternatives are unlikely. If the lenses are prolate rather than oblate, then the bands for tungsten must be rather different from those for molybdenum in this region. The broad range of evidence for all other sections in tungsten having isomorphs in molybdenum makes this possibility implausible at best.

In order that the nonobservance of the lens surface in tungsten may be shown to be due to its nonexistence (unoccupied states), it is necessary to rely upon the isomorphism of the tungsten and molybdenum Fermi surfaces. This is done by applying the two nearly-free-electron intersecting spheres model to the tungsten-neck data.

The areas of the neck orbits in the (001) plane of tungsten are plotted versus orientation in Fig. 5(a). As in the case of molybdenum (isomorphism applied here), one approximates the total area of the lens and neck orbits with the expression $A_0-B_0\cos 2\theta$. In tungsten,

however, no areas corresponding to the lenses along ΓH were observed.

If the initial assumption is that the missing lens in tungsten is spherical in form and quite small (and therefore contributes only a small constant term to the total area), a reasonable fit of the trial expression to the neck-orbit areas alone might be expected. The result is shown in the upper set of open circles in Fig. 5(a) where $A_0-B_0\cos 2\theta$ has been fitted to the neck area at [100] and [110]. The fit is seen to be less than satisfactory with respect to the angular variation of the neck area.

An equally plausible assumption is that the total area *must* be of the form $A_0-B_0\cos 2\theta$. Since the lens area would be relatively slowly varying near [110], the values for the area of the neck along could be used to represent the slope $dA/d\theta$ of the trial function. The difference between the trial function, fitted to the slope of the neck area near [110], and the measured values of the neck area over the remainder of the plane would then be proportional to the missing lens orbit area, plus or minus a constant term.

The results of this procedure are: $A_0\cong 0.1595$ Å^{-2}, $B_0\cong 0.1755$ Å^{-2} for the (001) plane [Fig. 5(a)] and $A_0\cong 0.1805$ Å^{-2}, $B_0\cong 0.155$ Å^{-2} for the $(0\bar{1}1)$ plane [Fig. 5(b)]. The function $A_0-B_0\cos 2\theta$ is shown as double open circles in Figs. 5(a) and 5(b) for the respective values of A_0 and B_0.

The average values for A_0 and B_0 give $R_a^2+R_b^2\cong 0.115$ Å^{-2}. If the observed value for the sphere orbit area at [100] is used for R_b^2, then $R_a\cong 0.208$ Å^{-1}. The distance between the centers of the two intersecting spheres is then D_a+D_b, where $D_a\cong 0.201$ Å^{-1} and $D_b\cong 0.255$ Å^{-1}. The resulting geometry is shown in Fig. 5(c).

TABLE III. Empirical Fermi-surface parameters for W and Mo.

Surface	Detail	Tungsten	Molybdenum
Jack and Lenses	Spheroid radius	0.263 Å^{-1}	0.365 Å^{-1}
	Spheroid length	0.580 Å^{-1}	0.730 Å^{-1}
	Oct. edge length	~0.93 Å^{-1}	~1.1 Å^{-1}
	Oct. point radius	0.21 Å^{-1}	0.186 Å^{-1}
	D_a	0.208 Å^{-1}	0.059 Å^{-1}
	D_b	0.255 Å^{-1}	0.324 Å^{-1}
	Neck diameter	0.272 Å^{-}	0.383 Å^{-1}
	Lens diameter	(not observed)	0.32 Å^{-1}
	Neck m^*	0.3 ± 0.03	0.445 ± 0.005
	Lens m^*	(not observed)	0.445 ± 0.005
	Spheroid m^*	0.505 ± 0.01	~0.5 (not observed)
	Lens-Neck gap	~0.32 eV	0.096 ± 0.002 eV
	Neck orbit g factor	$3.33\leq g\leq 4.0$	$2.22\leq g\leq 3.33$
	Estimated surface area	~8.6 Å^{-2}	~14.4 Å^{-2}
	Estimated volume	~0.88 Å^{-3}	~1.8 Å^{-3}
Holes at N	Axes		
	100	0.195 Å^{-1}	0.39 Å^{-1}
	110	0.146 Å^{-1}	0.30 Å^{-1}
	110	0.125 Å^{-1}	0.23 Å^{-1}
	(E_N-E_F)	0.284 ± 0.02 eV	0.81 ± 0.05 eV
	Estimated surface area	~1.70 Å^{-2}	~7.2 Å^{-2}
	Estimated volume	~0.09 Å^{-3}	~0.71 Å^{-3}
Holes at H	Extremal ⟨100⟩	1.436 Å^{-2}	...
	areas ⟨110⟩	1.067 Å^{-2}	
	⟨111⟩	0.99 Å^{-2}	1.037 Å^{-2}
	Length of Octahedron edge	~1.234 Å^{-1}	~1.264 Å^{-1}
	Estimated surface area	~5.26 Å^{-2}	~5.53 Å^{-2}
	Estimated volume	~0.85 Å^{-3}	~0.95 Å^{-3}

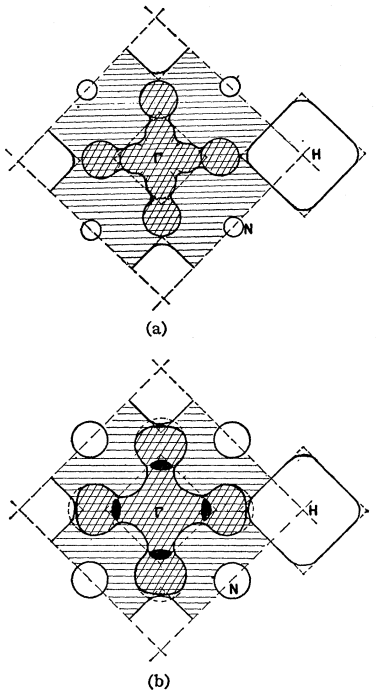

FIG. 6(a). Tungsten. Scale diagram of the semiquantitative model developed for tungsten. The dashed lines represent the simple figures used in the semiquantitative fit. The solid line figures are an artist's conception of the actual Fermi-surface geometry. (b). Molybdenum. Scale diagram of the semiquantitative model developed for molybdenum. The dashed lines represent the simple figures used in the fit to the data. The solid line figures are an artist's conception of the actual Fermi surface geometry.

The fact that "negative area" is required of the missing lens means that band five (the lens) is not an occupied band [see Fig. 5(c)]. The energy gap between the neck and the lens is: $\Delta E=0.32$ eV.[34] This crude estimate of ΔE is only 25% lower than the value determined by comparing the experimentally observed gap[5] between the jack and the octahedron with a theoretical gap.[31] Therefore, the value $\Delta E=0.32$ eV for the energy gap between band three (neck) and band five (lens) is tentatively identified with spin-orbit coupling effects. The fact that the gap due to spin-orbit coupling is larger in tungsten than in molybdenum is consistant with the fact that the g values for neck orbits in tungsten are larger than those for molybdenum.

Summary

The interpretation of the data has now proceeded to a point where semiquantitative models of the Fermi

[34] Since $\Delta A\text{gap}=(A_{\text{neck}}-A_0-B_0)$ and m^* is 0.3 for the neck. This is again a rigid-band approximation.

sembled. The geometrical parameters estimated in the preceding paragraphs have been collected in Table II.

The dashed lines of Figs. 6(a) and 6(b) are scale representations ($\Gamma H = 2.00$ Å^{-1}) of the simple figures used to approximate the Fermi surfaces. The solid line figures represent an artist's conception of the actual Fermi surfaces, based on the interpretation of the data presented above.

The results, in whole or in part, of many experiments have been used in arriving at the entries of Table III, and these results are in turn implied by the models. However, the total surface area, as determined by anomalous skin effect measurements in polycrystalline samples, and the required compensation of holes and electrons have not been incorporated in the development of the models. These two features are therefore taken as a test of the semiquantitative models of Figs. 6(a) and 6(b). The comparison is shown in Table IV.

Thus, these semiquantitative models of the Fermi surfaces of tungsten and molybdenum are precise to $\pm 10\%$.[35]

TABLE IV. Comparison of data with models.

Compensation of holes and electrons		
	Tungsten	Molybdenum
Total electron vol. (V_e)	0.88 Å^{-3}	1.8 Å^{-3}
Total hole vol. (V_h)	−0.94 Å^{-3}	1.65 Å^{-3}
Uncompensated vol. ($V_e - V_h$)	−0.06 Å^{-3}	0.15 Å^{-3}
$100(V_e - V_h)/(V_e + V_h)$	~3%	~5%
Number of carriers/atom	0.25	0.44
Total Fermi-surface area		
	Tungsten	Molybdenum
Model surface area	~16.0 Å^{-2}	~27.0 Å^{-2}
Experimental surface Area (see Ref. 1)	~18.0 Å^{-2}	~19.0 Å^{-2}
Difference	~2.0 Å^{-2}	~8.0 Å^{-2}
% Difference	~10%	~30%

IV. CONCLUSION

Experimental information concerning the Fermi surface of tungsten and molybdenum has been obtained from torsion measurements of the dHvA effect. This information consists of extremal areas of the Fermi surface and, in part, their related cyclotron effective masses. Where a direct comparison can be made, agreement with the results of other investigations is found.

The interpretation of the results of these torsion dHvA measurements in terms of the revised Lomer model of the Fermi surface shows excellent qualitative agreement. A semiquantitative model was developed which was shown to be compatible with the compensation of carriers, connectivity of surfaces, total surface area, extremal dimensions, and cyclotron effective masses reported by the authors and others.

Note added in proof. Recent augmented-plane-wave energy-band calculations for W and Mo, [T. L. Loucks, Phys. Rev. Letters **14**, 693 (1965); Phys. Rev. **139**, A1181 (1965)] are in substantial agreement with the revised Lomer model and the experimental results.

ACKNOWLEDGMENTS

We are grateful to W. A. Reed for arranging the loan of the high-purity tungsten and molybdenum samples, to J. H. Condon for many elightening discussions concerning both theoretical and technical details of the work, and to W. M. Walsh, Jr., and L. Mattheiss for discussions of their work prior to publication. Many points of interpretation were also clarified during discussions with J. A. Rayne, A. V. Gold, and E. Fawcett.

[35] The 30% difference in surface area between the model and the anomalous skin effect results is not considered relevant since either result carriers nearly the full difference as an error bar.